RESEARCH ARTICLE

Investigating the Mechanical Properties and Flexibility of N-BAR Domains in PICK1 by Molecular Dynamics Simulations

Shenghan Song¹, Tongtong Li¹, Amy O. Stevens¹, Taha Raad¹, Yi He^{1,*}

¹Department of Chemistry & Chemical Biology, The University of New Mexico, Albuquerque, New Mexico 87131, USA

ARTICLEHISTORY

Received: December 14, 2022 Revised: March 09, 2023 Accepted: April 14, 2023

10.2174/1389203724666230522093842

Abstract: The proteins of the Bin/Amphiphysin/Rvs167 (BAR) domain superfamily are believed to induce membrane curvature. PICK1 is a distinctive protein that consists of both a BAR and a PDZ domain, and it has been associated with numerous diseases. It is known to facilitate membrane curvature during receptor-mediated endocytosis. In addition to understanding how the BAR domain facilitates membrane curvature, it's particularly interesting to unravel the hidden links between the structural and mechanical properties of the PICK1 BAR domain. Methods: This paper employs steered molecular dynamics (SMD) to investigate the mechanical properties associated with structural changes in the PICK1 BAR domains. Results: Our findings suggest that not only do helix kinks assist in generating curvature of BAR domains, but they may also provide the additional flexibility required to initiate the binding between BAR domains and the membrane. Conclusion: We have observed a complex interaction network within the BAR monomer and at the binding interface of the two BAR monomers. This network is crucial for maintaining the mechanical properties of the BAR dimer. Owing to this interaction network, the PICK1 BAR dimer exhibits different responses to external forces applied in opposite directions.

Keywords: MD simulation, N-BAR domain, Mechanical properties, Helix kink, Curvature key residues

1. INTRODUCTION

The bending of the cell membrane is a microphysical process involved in endocytosis, exocytosis, and intracellular transport. A key step in these cellular biochemistry processes is the formation of tiny cell vesicles.[1, 2] A group of proteins with curved shapes is required to remodel the cell membrane.[3, 4] In many cellular processes, the proteins that facilitate the bending of the cell membrane are proteins containing Bin/Amphiphysin/Rvs167 (BAR) domains. The BAR acronym originates from three representative members in the protein family: mammalian Bin1, Amphiphysin, and yeast Rvs167.[5-7] Members of this protein family are frequently involved in membrane bending and remodeling in various cellular processes. BAR domains also play roles in physiological and pathophysiological conditions such as endocytosis, exocytosis, phagocytosis, and pinocytosis, among others. [8-13] Today, BAR dimers are known to be implicated in many diseases and disorders, including neurological diseases, developmental disorders, and even

Alzheimer's disease.[14] Therefore, gaining an in-depth understanding of how the BAR domains contribute to the formation of membrane curvature and vesicle generation is not only a matter of scientific curiosity but also a step toward advancements in modern physiology.

BAR domains perform their biological functions in the form of dimers and often form even higher-level aggregates. The N-BAR domain, a subfamily of the BAR domain, forms a dimer with a crescent shape. N-BAR domains have been found in various proteins, including Amphiphysin, endophilin, and Protein Interacting with C-Kinase 1 (PICK1). N-BAR domains bind to the membrane via positively charged residues located on its concave surface. [15] In addition to the positively charged concave surface, N-BAR domain proteins also contain an N-terminal amphipathic helix. Existing experimental results demonstrate that the rigid concave shape, the positively charged concave surface, and the N-terminal amphipathic helices are all crucial for the N-BAR domain's ability to bend and remodel the cell membrane. [16–22]

All-atom Molecular Dynamics (MD) simulations are powerful tools to probe the structural and dynamical properties of proteins at residue or atomic resolution.[23–32]

^{*}Address correspondence to this author at the Department of Chemistry & Chemical Biology, The University of New Mexico, Albuquerque, New Mexico 87131, USA; Email: yihe@unm.edu

They can complement novel experimental techniques which are limited by resolution, size, and complexity to explore the finer details of the N-BAR systems. Previous work has taken advantage of the benefits of MD to simulate BAR domains. The MD simulations by Blood et al. exemplified that Drosophila Amphiphysin N-BAR domains can shape the membrane surface into the curvature of the BAR domain.[33] In follow-up work, they revealed that the characteristics of N-BAR, such as the positively charged convex surface, the rigidity and orientation of the overall structure, and even the presence or absence of N-terminal helices, all greatly affect the ability of the BAR dimer to bend the membrane.[34]

Until now, most simulation studies have focused on the membrane-bending process of the N-BAR dimer. However, the mechanical properties of the N-BAR dimer, in particular, the rigidity and flexibility of the N-BAR dimer, hold the key to understanding how the BAR domains perform that function. The goal of this paper is to use all-atom MD simulations to investigate the degree of flexibility and rigidity of a BAR monomer (within a dimer form) and the stability of the helical structure of the BAR monomers under external forces. We performed Steered Molecular Dynamics (SMD) simulations in which external forces were applied to a single BAR monomer within the BAR dimer while restraining the other monomer. As shown in Fig. (1), we applied upward and downward external forces (positive and negative directions along the Y-axis) to probe the different responses of the BAR domain monomers to external forces from different directions. We observed that the PICK1 N-BAR monomers undergo unique structural changes when subjected to external forces in different directions. Our results suggest that the PICK1 BAR domains are more resistant to upward external forces (positive direction of the Y-axis), which corresponds to the state when it performs its biological functions. In addition, the breakdown of the helical structure of the N-BAR domain monomer showed a strong preference in specific residue regions. Our results provide an in-depth understanding of the BAR domain which can serve as a theoretical basis for future engineering of the BAR domain.

2. MATERIALS AND METHODS

2.1 Systems of Molecular Dynamics Simulations

The starting structure of the simulations for the N-BAR dimer of PICK1 was created by Han. D. et al, as shown in Fig. (1)[35]. This structure has been previously used to explore the inter-domain dynamics of PICK1.[32] The PICK1 BAR dimer was modeled using Arfaptin[36] and Endophilin[21] as templates. Using proteins from same subfamily as templates is considered a reliable method for predicting the structure of the dimer for several reasons. Firstly, the PICK1 BAR domain has a high sequence identity with the N-BAR domain protein Arfaptin-2, which provides a robust foundation for modeling the structure of the PICK1 BAR dimer. Secondly, the high structural similarity between the Arfaptin-2 BAR dimer and Endophilin lends additional support for the model's reliability, as Endophilin is a well-studied N-BAR domain protein that

has been extensively characterized in the past. This structure includes only residues 144 to 357, as these residues are closely related to the reshaping the membrane. To mimic the cellular environment, the steering simulations of the N-BAR dimer were conducted in a system with explicit water molecules. The TIP3P water molecule was used to solvate the systems. [37] The CHARMM36 force field was used in all simulations. It was generated by CHARMM-GUI [38, 39] and visualized using visual MD (VMD) and Chimera. [40, 41] A solvation box measuring 27×27×27 nm³ was used to accommodate PICK1 N-BAR dimer (~13 nm for monomer) and provide adequate space for the deformation of the BAR monomer. All systems were neutralized with counter ions. The system building process, which includes adding water molecules, ions, and placing the N-BAR domains, was conducted using the GROMACS software package [42, 43]. The number of trajectories and simulation timescales are presented in Table 1. All systems were minimized to a maximum of 50,000 steps to remove non-physical contacts and interactions. Subsequently, an NPT ensemble with 50,000 steps was executed to equilibrate the systems. After conducting 50,000 steps of energy minimization and NPT equilibrium dynamics simulations, the root mean square deviation (RMSD) of the BAR Dimer during the NPT simulation was calculated, as shown in Fig. (S1a). To assess the efficiency of the equilibrium simulations, the simulations were extended to 1 ns and 10 ns, and the RMSD was calculated, as shown in Fig. (S1b). In the 100 ps, 1 ns, and 10 ns NPT simulations, the RMSD of the BAR Dimer was approximately 0.04 nm, indicating that the configuration of the BAR Dimer reached equilibrium at the end of 100 ps and is suitable for subsequent simulations. The LINCS algorithm was utilized to constrain bond lengths between heavy atoms and hydrogen atoms. [44] Simulations were conducted at a constant temperature of 310 K, as reported in previous work, to replicate the cellular environment. [33, 34] A constant pressure of 1 atm was maintained using the Perriello-Rahman method. Periodic boundary conditions were implemented in all three directions, and the Particle Mesh Ewald (PME) method was employed. [45-47] The cutoff distance of both the van der Waals interaction and Coulomb interaction was set to 14 Å. In all pulling simulations, external forces were applied to the center of mass of Chain B of the PICK1 N-BAR dimer. Structural restraints were applied to Chain A. Since the PICK1 N-BAR dimer is symmetric, we only studied the flexibility and rigidity of Chain B under external forces, which can represent the common behavior of the two chains. The constant velocity pulling simulations were performed at pulling rates of 4 nm/ns, 1.6 nm/ns, and 0.8 nm/ns. The N-BAR dimer was subjected to both upward and downward external forces. Residue distances and angles were calculated using the modules in GROMACS. In all pulling simulations, the moving distance of the center of mass of Chain B of the N-BAR domain was approximately 8 nm. The pulling simulations with rates of 4 nm/ns and 1.6 nm/ns were repeated 10 times in both directions. The pulling simulations with the rate of 0.8 nm/ns were repeated twice in both directions.

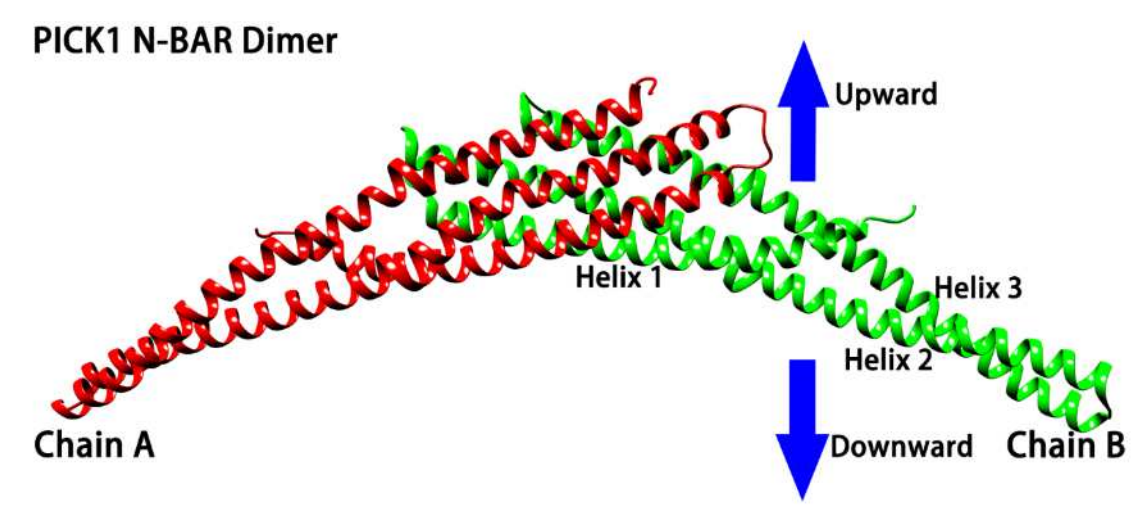


Fig. (1). Schematic diagram of steered molecular dynamics simulations. Red is the monomer Chain A. Green is the monomer Chain B. Each monomer has three helices, denoted as Helix 1, Helix 2, and Helix 3, respectively. (A higher resolution/colour version of this figure is available in the electronic copy of the article).

2.2. Time-resolved Force Distribution Analysis

The time-resolved force distribution analysis was conducted using the Time-resolved Force Distribution Analysis (TRFDA) software package, in conjunction with GROMACS. [48] In TRFDA, residue-based pairwise forces for Coulomb and Van der Waals interactions were computed and observed over the course of the simulation. The interaction between residue i and residue j is depicted by a pairwise force, which can be calculated using the sum of the atom-based pairwise forces between residues i and j. The details of the pairwise force calculations are described in a separate paper. [49]

2.3. Interaction Area, Secondary Structure Analysis and Helix Kink

The interaction area's calculation and the secondary structure analysis of Chain B were completed using the GROMACS module. [50] Even though GROMACS does not have a direct module for computing the interaction area, the *gmx sas* [51] module was employed to calculate the solvent-accessible surface area, which can then be used to derive the interaction area using the following equation (1).

$$S_{Interaction} = \frac{SASA_A + SASA_B - SASA_{A\&B}}{2} \tag{1}$$

The secondary structure analysis of Chain B in the BAR domain was conducted using the *do_dssp* module in GROMACS. [52] The results of the analysis were subsequently processed and visualized using the GNUplot software.

The *Kink Finder* [53] software package was utilized to identify all helical kinks in the three helices of Chain B in the BAR domain. This software pinpoints all the kink residues in

a chain and the torsional angle of each helix bend at every kink. More details on *Kink Finder* can be found in the original paper. [53]

Table 1. Number and time length of simulation systems.

Direction	Time (ns)	Number of Trajectories			
Upward	0.5	10	5		
	2	10	20		
	5	10	50		
	10	2	20		
Downward	0.5	10	5		
	2	10	20		
	5	10	50		
	10	2	20		

3. RESULTS

3.1. Structure Changes in BAR Domain Structure Under External Force

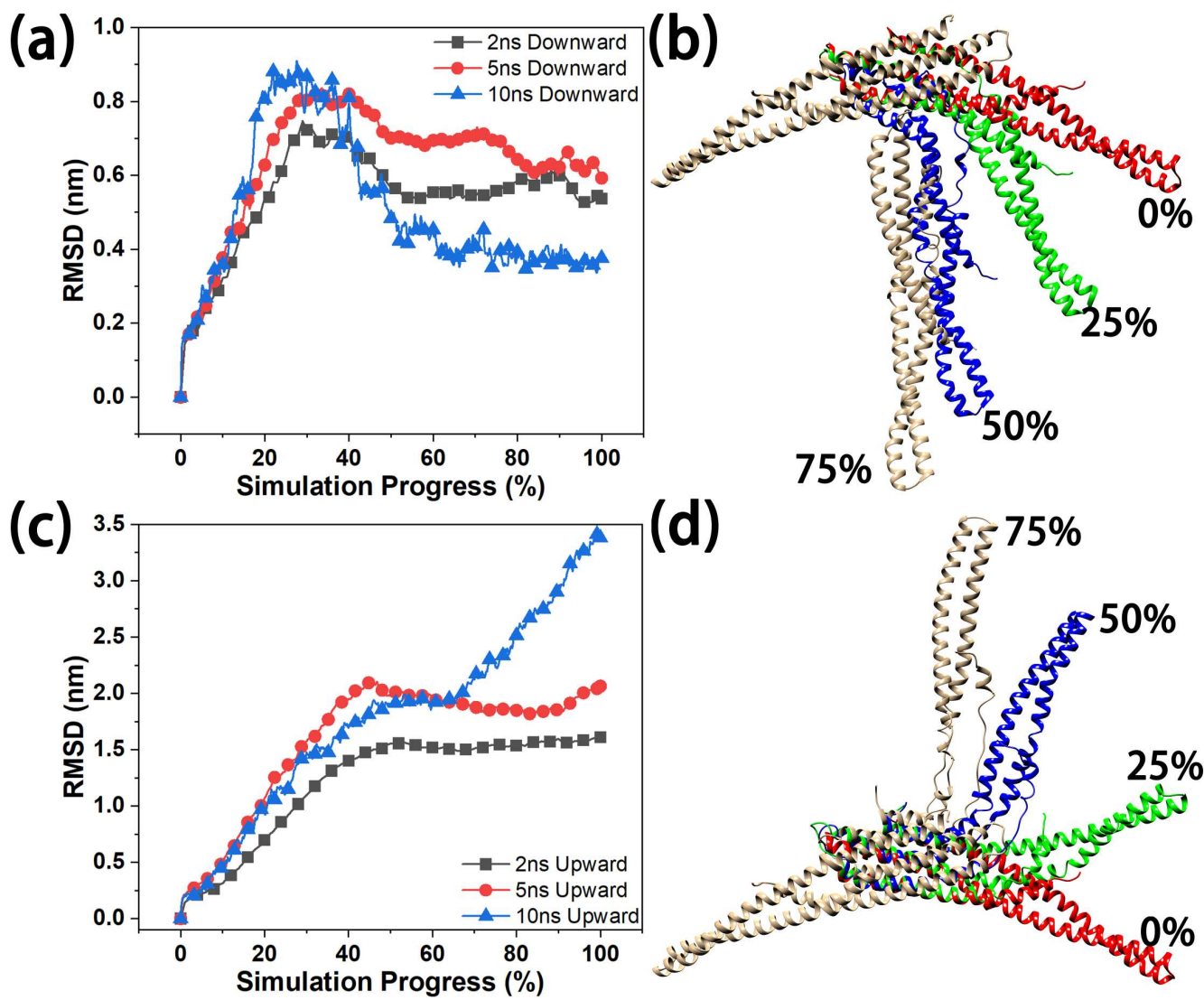


Fig. (2). Root mean square deviation (RMSD) during pulling simulations, and molecular structures at four distinct time-points for steering progress of 0%, 25%, 50%, and 75%. (a) and (b) Downward SMD simulations. (c) and (d) Upward SMD simulations. The results of the RMSD calculations shown above are averaged over all trajectories with the same time scale. (A higher resolution/colour version of this figure is available in the electronic copy of the article).

Following the completion of the simulations, we calculated the root mean square deviation (RMSD) of Chain B of the BAR domain to explore the structural changes in the N-BAR domain under external forces. The root mean square deviation (RMSD) of Chain B is shown in Figs. (2a and 2c). The maximum RMSD in downward-steering simulations reaches 0.9 nm in the 10 ns simulation system. Furthermore, downward systems with different pulling speeds yield similar RMSD results. The 5 ns pulling simulation system was chosen as the representative case for the downward-pulling simulations. To highlight time-dependent changes, four time-points were selected for analysis, corresponding to pulling progress of 0%, 25%, 50%, and 75%. Fig. (2b) depicts the structures of Chain B at these four time-points. It can be

observed that the structure of Chain B does not significantly change during the simulation process, with a maximum of 0.9 nm. In contrast, the maximum RMSD is 1.5 nm for the 2 ns upward-pulling simulation, as illustrated in Fig. (2c). Intriguingly, the maximum RMSDs for the 5 ns and 10 ns upward-pulling simulations are approximately 2.2 nm and 3.5 nm, respectively. The upward-pulling simulations not only cause significant changes to the structure of Chain B but also result in the disappearance of part of the helical structure, as shown in Fig. (2d). According to the RMSD, the 5 ns and 10 ns upward-pulling simulations produce similar outcomes. Consequently, only the 2 ns and 5 ns upward-pulling simulation systems were utilized to analyze the pulling process and structural changes in depth.

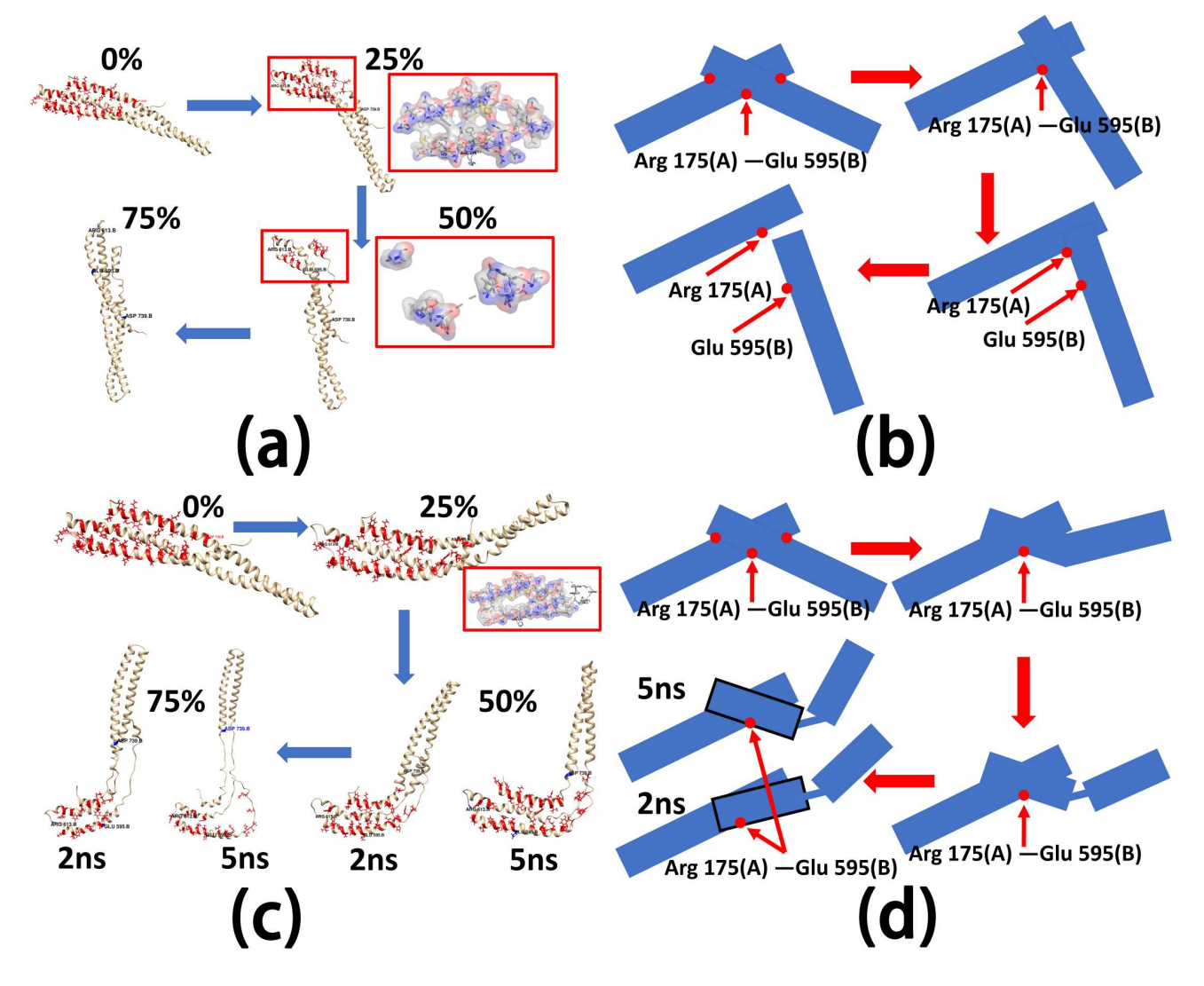


Fig. (3). Changes in the structure of the PICK1 N-BAR dimer during the steering simulations. Among them (a) and (c) are representative structures for these time-points, (b) and (d) are simplified schematic diagrams. (a) and (b) are downward-pulling SMD simulations, while (c) and (d) are upward SMD-pulling simulations. (A higher resolution/colour version of this figure is available in the electronic copy of the article).

The change in the number of hydrogen bonds can accurately reflect alterations in interactions between residues. We have calculated the number of hydrogen bonds within the BAR monomer and between the monomers to trace the evolution of these interactions (See Fig. (S2)). The number of hydrogen bonds in Chain B initially decreases before it starts to increase (as represented by the black curve). The majority of hydrogen bonds in the monomer occur within the helices.

With this data in mind, the fluctuations in the number of hydrogen bonds signify the vanishing and reformation of helices throughout the pulling process. The red curve in Fig. (S2) displays the number of hydrogen bonds between Chain B and Chain A during these pulling procedures. As the pulling advances, the quantity of hydrogen bonds between Chain B and Chain A eventually falls to zero. This suggests that the

interaction between Chain A and Chain B progressively weakens until it ultimately disappears. Regardless of the duration of the upward system (2 ns, 5 ns, or even 10 ns), the count of hydrogen bonds in Chain B plummets rapidly. This kind of alteration in the number of hydrogen bonds implies that the upward external force has instigated the deformation of the helices in Chain B. When considering the number of hydrogen bonds between Chain A and Chain B (as shown by the red curves in the top panels), different simulation times yielded varying results. Coupled with the conformational change of Chain B under the application of external forces, in the 2 ns pulling simulation, the external force is rather large, and ultimately, Chain B and Chain A become completely separated. This causes the count of hydrogen bonds to fall to zero. In the 5 ns and slower steering simulations, the external force is less intense. Although the external force drives Chain

B upward, the smallest helix in Chain B consistently maintains interactions with Chain A. This action prevents the number of hydrogen bonds between Chain B and Chain A from reaching zero during the final phase of the simulation. According to the results of RMSD and hydrogen bonds, it is clear that the BAR domain has responded differently to external forces applied in different directions, resulting in diverse structural changes.

3.2. Upward and Downward Pulling Processes

Using LigPlus[54], we explored all the contact pairs between two BAR monomers in a dimer. As can be seen in both Fig. (3a) and the "Structural Properties of BAR Domain" section in the Supporting Information (SI), we identified the three most important residue pairs: Arg175(A)-Glu595(B), Glu155(A)-Arg613(B), and Arg197(A)-Asp739(B). As shown in Figs. (3a and 3b), after 25% of the downwardpulling simulation progressed, two representative interaction residue pairs disappeared (Glu155(A)-Arg613(B) and Arg197(A)-Asp739(B)), leaving only one pair (Arg175(A)-Glu595(B)). In contrast, the number of hydrophobic interactions between the two chains remained stable. These results indicate that the downward external force caused Chain B to rotate slightly around the residue pair Arg175(A)-Glu595(B). When the simulation progress reached 50%, the hydrophobic interactions were significantly reduced compared to the 25% time-point (as shown in Fig. (3a) bottom right panel). It should be noted that the residue pair Arg175(A)-Glu595(B) also broke at this stage. At this point, two monomers were about to separate. At 75% time-point, there was almost no interaction between the two chains, which suggested that the downward force had led to the separation of Chain A and Chain B. In addition, Chain B, which had an obvious bend in the previous phase of the downward-pulling simulation, had also returned to a straight state.

For the upward-pulling simulation (shown in Figs. (3c and 3d)), after 25% of the simulation progress, there was almost no change in the residue interactions between Chain A and Chain B (as shown in Fig. (3c) upper panels). However, the upward force caused Chain B to curve significantly. With the upward external force continuing to act on Chain B of the BAR domain, only the tail region of Chain B continued to move upward. When the simulation progress reached 75%, the number of residues in Chain B interacting with Chain A was significantly reduced. Although the helix structure in the middle region of Chain B had basically disappeared, the bundle of three helices remained intact. As a whole, the upward movement of Chain B was more pronounced.

To extract more detailed information on the bending process, we used the interaction area to illustrate the changes in the interaction between the two monomers of the BAR dimer. The interaction area between the two chains was calculated for the pulling simulations under three different time scales, as shown in Figs. (4a-4c). The black line represents the interaction area in the upward-pulling simulations, while the red line represents the interaction area

in the downward-pulling simulations. A larger interaction area indicates more interacting residues, a stronger interaction, and tighter binding between Chain A and Chain B.

As the downward-pulling progresses, the interaction area gradually decreases. This indicates that the number of interacting residues between Chain A and Chain B also decrease. The consequences of this reduction are that the binding between the two monomers weakens, and the opening angle of the BAR dimer changes more easily. Interestingly, the upward-pulling simulation yields different results. Even though the upward external force acts on Chain B, the interaction area increases instead of decreases. Table S1 illustrates the number of interacting residue pairs between Chain A and Chain B of the PICK1 BAR dimer in its native state and at 25% time-point, both upward and downward. During the downward-steering, all 67 residue pairs in the native state break, generating 17 new pairs of interacting residues. In contrast, upward-steering not only maintains 60% (35 out of 67) of the residue pairs in the native state but also generates 23 new interacting residue pairs. The process of pulling Chain B up is accompanied by the generation of more new interacting residue pairs. The newly formed residue pairs compensate for the energy change during upward rotation while also binding the two monomers more tightly. Such a scenario leads to structural changes in the mid-section and tip of the BAR monomer. Downward rotation breaks all interacting residue pairs at the interface of the native PICK1 BAR dimer and generates fewer new interacting residue pairs. The binding between the two monomers weakens due to the significant reduction in the pairs of interacting residues. The external force required to rotate downward will also decrease. This is consistent with the upward-pulling and rotating process of Chain B described in the first section and the calculation results in Tables S1 and S2 in the Supporting Information (SI). As shown in Fig. (S7), the punctual stress observed in TRFDA results also confirms the discussion on the external force above. In summary, the peculiar crescent structure of the PICK1 N-BAR dimer results in a striking difference in how it behaves when subjected to upward and downward external forces.

Yu et al. [55] and Mahmood et al. [56] both performed molecular dynamics simulations of the BAR dimer interacting with and bending the membrane. They used the opening angle [55] and RMSD [56] of the BAR dimer to describe the structural changes of the BAR domain. In the biological process of the BAR dimer bending the membrane, the BAR domain will receive upward pressure from the membrane. This is similar to the upward external force we applied to the BAR domain. Their simulations have proven that the BAR dimer undergoes no obvious opening angle changes in the process of bending the membrane. In other words, it is more difficult to change the opening angle of the BAR dimer using the upward external force. This is consistent with our results. We also find that the core part of the BAR monomer has a large number of interactions across different chains and

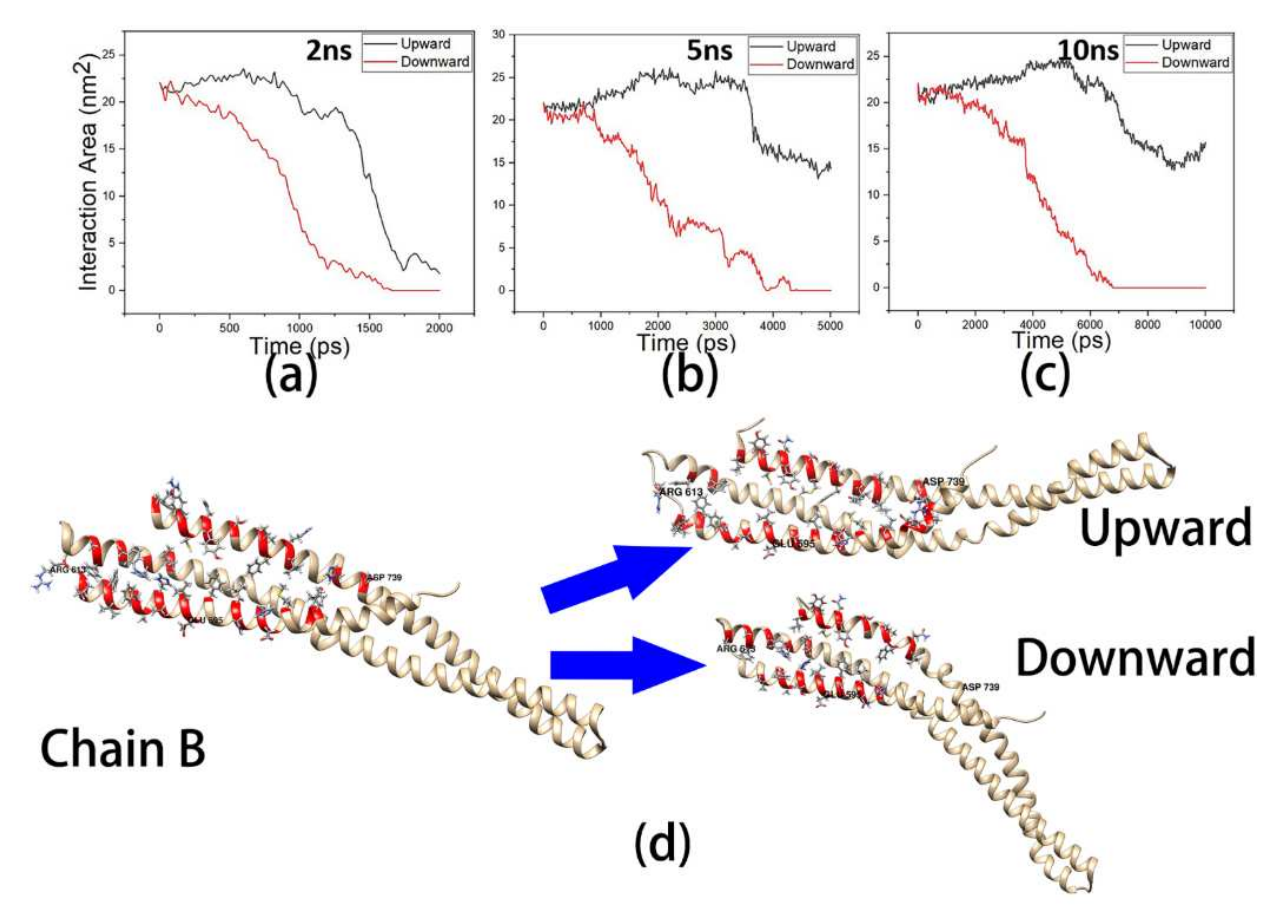


Fig. (4). The change of interaction area between two monomers. (a) 2 ns. (b) 5 ns. (c) 10 ns. (d) the bending structure of the monomer Chain B at the beginning of the upward and downward SMD simulations. Residues that interact with monomer Chain A are shown in red. (A higher resolution/colour version of this figure is available in the electronic copy of the article)

different helices, which contribute to the stability and rigidity of the dimer. However, the tip of the monomer possesses good elasticity and only mutually stable interactions between Helix 2 and Helix 3 (Fig. (S3c)). This allows the BAR domain monomer's tip to bend up or down around the equilibrium position under external forces. When a monomer (Fig. (4d)) is rotated downward by an external force while bending, the number of interacting residues decreases, which facilitates its deformation and changes the opening angle from the force aspect. Conversely, when an upward external force is applied, the monomer bends upwards. The upwardly curved part of the monomer forms new interactions with the core part of the other monomer in the dimer, resulting in an increase in the interaction area and residues. The newly formed interactions between monomers hinder the relative movement and rotation between the two monomers. This is to prevent further deformation of the dimer. In summary, the combination of the elasticity of the BAR monomer and the crescent shape of the BAR dimer forms the anisotropy of the external force of the opening angle of the BAR domain.

3.3. Structural Changes of the Three Helices of BAR Monomer Under External Force.

The internal changes within the BAR monomer under external forces are of particular interest to reveal the key residues that maintain the integrity of the BAR monomer. To obtain such information, we investigated the structural changes in each of the three helices under the action of upward and downward external forces. As shown in Figs. (4a - 4c), it is notable that Chain B of the PICK1 N-BAR domain has obvious anisotropy under the action of external force; that is, under the action of external force in different directions, Chain B behaves differently.

3.3.1. Interactions between Helices within the Monomer

As a protein domain with important biochemical functions, the structure of N-BAR domains is stable in an aqueous environment. The three helices can stabilize each other through various interactions. To explore the changes in these interactions, time-resolved punctual stress was calculated during the pulling process, as shown in Fig. (5). Punctual stress represents the sum of the force acting on each residue. With the TRFDA tool, atomic pairwise forces were calculated for interaction energy and monitored over simulation time.

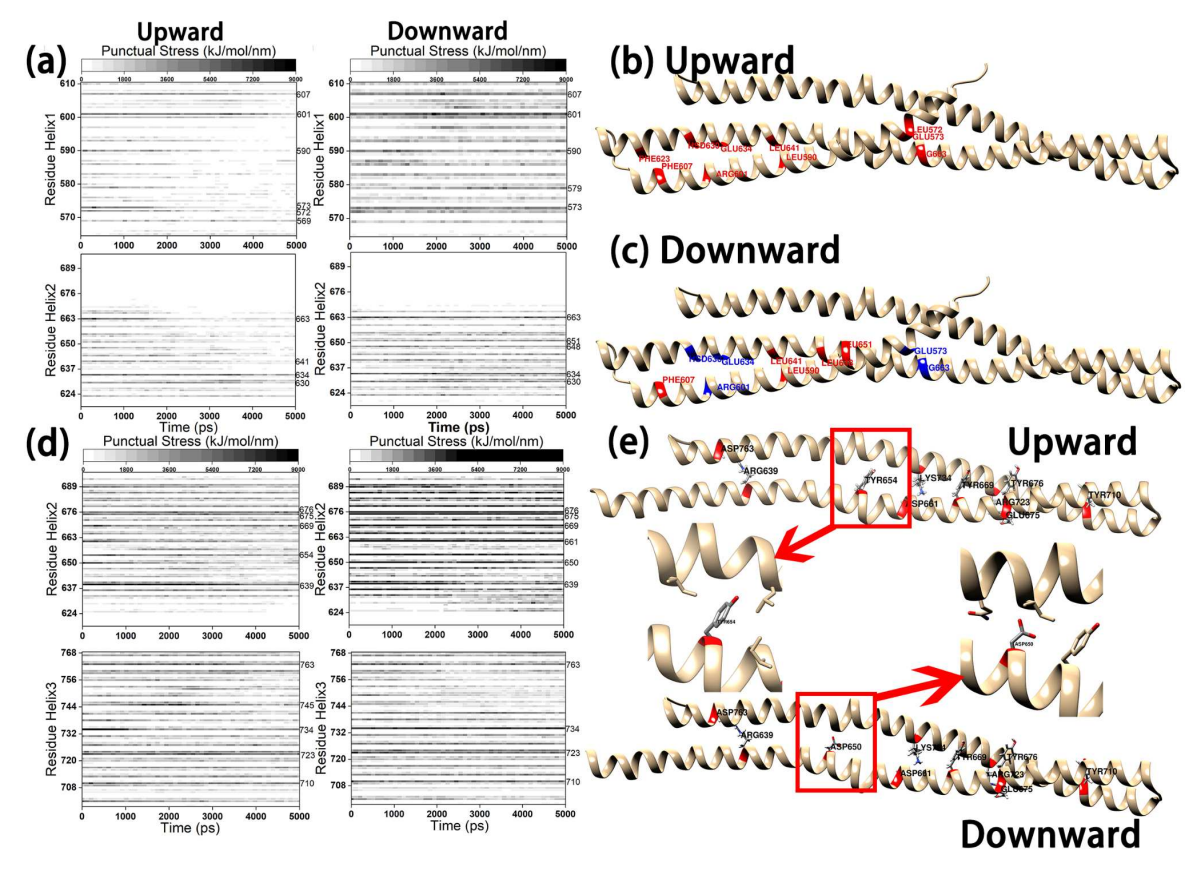


Fig. (5). Punctual stress according to TRFDA analysis. (a) Punctual stress from interactions between Helix 1 and Helix 2. (b) and (c) Key residues between Helix 1 and Helix 2 based on Punctual stress accumulation results. (d) Punctual stress from interactions between Helix 2 and Helix 3. (e) Key residues between Helix 2 and Helix 3 based on punctual stress accumulation results. The analysis for the steering process is from representative trajectories. (A higher resolution/colour version of this figure is available in the electronic copy of the article).

Table 2. Key residues in the upward and downward simulations between Helix1 and Helix 2, Helix 2 and Helix 3.

Key residue rank	Upward Helix 1-Helix 2		Downward Helix 1-Helix 2		-	Upward Helix 2-Helix 3		Downward Helix 2-Helix 3	
	2 ns	5 ns	2 ns	5 ns	2 ns	5 ns	2 ns	5 ns	
1	634	634	634	601	639	639	734	734	
2	601	601	601	634	734	723	639	669	
3	607	607	663	663	723	763	723	723	
4	630	630	607	607	763	676	675	661	
5	663	663	590	573	675	675	661	710	
6	572	573	648	630	710	734	710	639	
7	590	572	630	590	661	710	676	676	
8	573	569	651	648	669	669	669	675	
9	641	641	573	651	676	745	763	763	
10	623	590	641	579	654	654	650	650	

TRFDA can be used to track signal propagation at the atomic level, characterize dynamical intermolecular interactions, develop force fields, and conduct energy-based analysis. The interaction force results obtained by TRFDA are more accurate and sensitive, which aids in determining key residues. We initially analyzed the interaction between Helix 1 and Helix 2, as shown in Fig. (5a). The residues under the largest punctual stress were those interacting with the other helix. It should be noted that some residues alternately appear in dark and light colors, such as residues 601 and 590 in Helix 1 during the upward-pulling simulation. This indicates that, with the progress of pulling and the application of external forces, the interactions formed by these residues were deformed and then reformed. As Helix 1 is shorter than Helix 2 and concentrated in the core part of Chain B, the interactions between Helix 1 and Helix 2 play a crucial role in maintaining the stability of the core part of the BAR domain monomer.

Comparing the punctual stress of Helix 1 and Helix 2 during the upward and downward-pulling simulations, the most noticeable difference was observed in the upward-pulling simulations. Some residues on Helix 1 (approximately residues 573-600) initially experienced punctual stress during pulling. However, as the pulling continued, the punctual stress on these residues gradually decreased to zero. This suggests that the interactions between these residues and Helix 2 disappeared due to the upward external force. This finding aligns with the separation of Helix 1 and Helix 2 observed in our previous analysis in section 3.1. In the downward-pulling simulations, neither the direct analysis of the pulling process nor the calculation results of punctual stress indicated a separation between Helix 1 and Helix 2.

Fig. (5d) displays the specific stress generated by the interaction between Helix 2 and Helix 3 of the BAR domain monomer. Dynamic interactions exist between Helix 2 and Helix 3, distributed at the interface of the two helices. Notably, key residues exhibit higher punctual stress than other residues. Table 2 lists the ten residues with the highest specific stress. While there are some differences in ranking order, 8 out of the 10 key residues remain consistent in the upward and downward-pulling simulations. This implies that these residues play a vital role in the interaction between Helix 2 and Helix 3. Among these key residues, charged amino acids comprise about 60%. These key residues bind Helix 2 and Helix 3 tightly through hydrogen bonding and electrostatic interaction. Interestingly, despite exerting substantial specific stress, some key residues are relatively isolated compared to others. These residues form an interactive residue network with several surrounding residues through hydrophobic and electrostatic interactions. Due to interactions with multiple residues, they often exhibit larger specific stress.

In addition to the ten residues with the highest specific stress, other residues also contribute to interactions between the two helices. These residues form a dynamic interaction network between the two helices through numerous hydrogen bonds, hydrophobic interactions, and electrostatic interactions, as shown in Fig. (S6a). When an external force is applied, the relative positions of Helix 2 and Helix 3 change. This process involves the breaking and formation of interactions between various residues. The residue-residue interactions resist breaking in response to the pulling force, maintaining the helical structure of Helix 2 and Helix 3. Evidently, the disruption of these interactions opposes the external forces, thereby preserving the helical structure of Helix 2 and Helix 3. Moreover, Helix 2 forms an interaction network with Helix 1 near the core, enabling the three helices in the BAR domain monomer to stabilize each other, resulting in a rigid core and a flexible tail. The interaction between Helix 2 and Helix 3 is concentrated between the two helices, indicating selectivity towards external forces from different directions. When subjected to an upward force, Helix 3 bends upwards. Concurrently, the residues located in the interaction network on the lower surface of Helix 3 move away from each other. This leads to the breaking of hydrophobic aggregation interactions and other interactions among residues, resisting the external forces.

3.3.2. Changes in the Secondary Structure under External Force

From our analysis of the pulling process, we found a significant difference between the upward and downward-pulling simulations. In the upward-pulling simulations, the external upward force induced numerous changes in the helical structure of Chain B in the secondary structures during the pulling process, as shown in Fig. (S5).

In contrast, the downward external force did not induce a significant change in the secondary structure of Helix 2. This difference suggests that the rigidity of Helix 2 is dependent on the direction of bending. For Helix 3, part of the helical structure changed regardless of whether the external force was upward or downward. It is worth noting that many of the residues involved in these structural changes are consistent when the external force causes changes in the helical structure of Helix 3. Interestingly, under the downward external force, the secondary structures around residues ALA658 and ILE644 of Helix 2 temporarily shifted from an α-helix to a turn. Similarly, in the upward-pulling simulation, the altered secondary structures were also located near residues ALA658 and ILE644. The secondary structure analysis indicates that regions of both Helix 2 and Helix 3 have helical structures significantly less stable than other regions. It's important to highlight that some residues within a helix can cause the α helix to bend. These residues that significantly cause the helix to bend are known as helix kinks, which are known to disrupt the structure of helices. Kink Finder[53] is a previously developed software utilized to identify the kink residues in helices. In our research, we used Kink Finder to identify helix kinks in Helix 2 and Helix 3, as shown in Fig. (S5). Changes in the secondary structure under the influence of external force are all located near the helix kinks identified using Kink Finder. Notably, some of the kink residues identified by Kink Finder are distinctly helix-forming amino acids. Consequently, we refer to the helical segment lacking hydrogen bonds as the kink region. The results of DSSP secondary structure analysis and kink analysis show that the existence of kinks reduces the rigidity of the helices, leading to changes in the helical structure in some regions under the influence of external force.

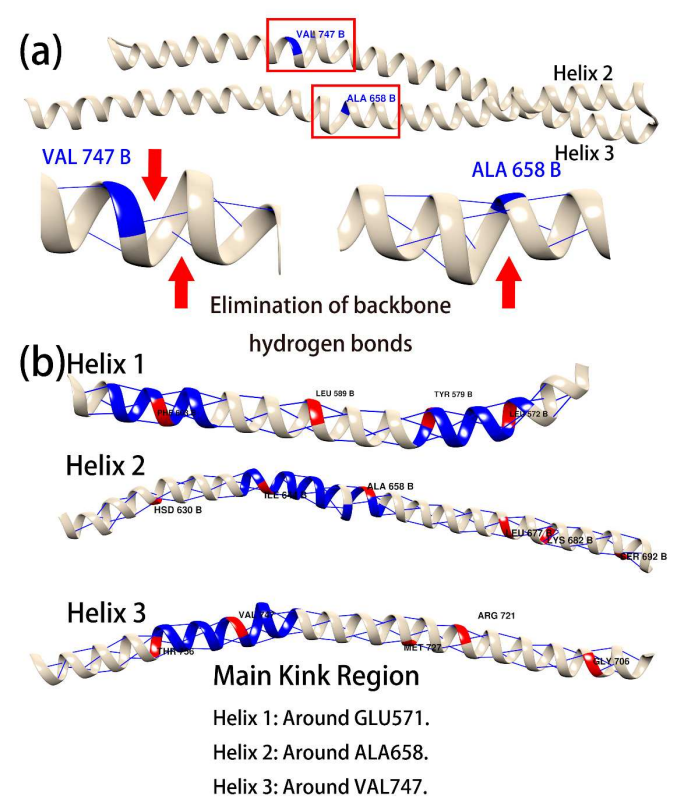


Fig. (6). The main kinks of the three helices of the monomer Chain B. (a) Main kinks on Helix 2 and Helix 3. (b) Kinks in all three helices. Blue residues are the segments that tend to lose secondary structure. (A higher resolution/colour version of this figure is available in the electronic copy of the article).

When subjected to upward and downward external forces, Helix 2 and Helix 3 exhibit different levels of rigidity. This is due to the presence of kink residues, which cause the helix to lose part of its hydrogen bonding network. The loss of hydrogen bonds makes a helix more likely to lose its helical structure when subjected to external forces. In addition, pinpoint stress and residue interaction patterns suggest extensive interactions between Helix 2 and Helix 3. These interactions can form a network located between Helix 2 and 3, providing additional support for the helices in a single direction, as shown in Fig. (S6b). These findings suggest that Helix 2 and Helix 3 display different levels of rigidity when subjected to external forces from different directions.

4. DISCUSSION

4.1. Interpretation of the Anisotropy of Helixes in Monomer Under External Forces

Based on the results of secondary structure analysis and the positioning of the helix kinks, the disappearance of the helical structure is closely tied to the kinks when exposed to external forces. In Fig. (6a), one can see that the helix kinks cause the helix to bend in a specific direction, eliminating the hydrogen bonds on the opposing side. Without these crucial hydrogen bonds to maintain the pitch of the α -helix (the vertical distance between consecutive turns of the helix), the helix bends. When the external force continues to act on the helices, the pitch between residues near the helix kink, which no longer participate in a hydrogen bonding network, will continue to increase.

As for Helix 2, the primary kink region (around ALA658) is situated on the upper side of the helix, causing Helix 2 to bend upwards. Simultaneously, the pitch beneath the main kink increases, and the hydrogen bond is broken. Regarding Helix 3, the primary kink region (around VAL747) is positioned on the front side of the helix. The helix kink prompts the helix to eliminate hydrogen bonds on both the upper and lower sides. The loss of hydrogen bonds makes it easier for Helix 3 to alter the helical structure at the kink area when it is subjected to both upward and downward external forces. However, due to the presence of the residue interaction network between Helix 2 and Helix 3, Helix 2 can provide additional support to Helix 3 when faced with an upward external force. As a result, Helix 3 exhibits greater rigidity in the upward-pulling simulation than in the downward-pulling one.

4.2. Influence of Kinks and Key Residues on the Flexibility of BAR Domain Monomers.

As shown in Fig. (S6), the results of the network analysis reveal that the structure formed by Helix 2 and Helix 3 can be divided into four segments. The adjacent helix segments of Helix 2 and Helix 3 share the same color, suggesting they have the same inherent movement tendency when subjected to external forces. This phenomenon correlates with the interaction patterns between Helix 2 and Helix 3.

Helix 2 and Helix 3 do not act as a unified whole but are rather divided into several segments. The division points of these helix segments align precisely with the locations of the kink residues. The key role of kinks in the helices of transmembrane proteins is discussed by T. Blundell et al., D. N. Langelaan et al., and E. C. Law et al. [57-59] Although kinks cause the helices of transmembrane proteins to bend and lose hydrogen bonds, they are vital functional and flexible points in helices. Kinks provide residue points that allow for conformational change and structural flexibility, making them often functionally important in proteins. P. D. Blood et al. conducted a simulation of the interaction between the N-BAR domain and the membrane. [34] They clearly observed that in the process of bending the membrane, the tail region of the N-BAR domain also bends and deforms. These deformations are essential for the N-BAR domain's ability to interact with the membrane. We believe that helix kinks are indispensable and vitally functional to the N-BAR domain. Moreover, in the

process of bending the membrane, the bending and deformation of the BAR domain itself hold significance. The kinks lower the free energy of the BAR domain's bending, making it easier to deform. Although kinks might decrease the rigidity of the helix of the BAR domain, they provide the BAR domain with curvature and flexibility for functioning. Therefore, the presence of kinks is conducive to the function of the BAR domain.

5. CONCLUSION

In this article, we performed a series of pulling simulations on the PICK1 N-BAR dimer. External forces of varying strengths were applied to a monomer (Chain B) of the BAR dimer, both in upward and downward directions. While the deformation of the BAR domain caused by pulling exceeds what can be achieved in biological systems, these extreme simulations allow for a clearer illustration of the impact of external forces on the BAR domain. A comprehensive understanding of the rigidity and flexibility of the BAR domain can help elucidate the mechanism behind the BAR domain's membrane-bending process. We found that there is a significant difference in the responses of the BAR domain depending on the directions of external force. This difference indicates the varying rigidity of the BAR dimer's opening angle when forces are applied upward versus downward. Both punctual stress and conformational results reveal that interactions exist not only between the two monomers but also within an interaction network between the helices of each monomer. This interaction network can maintain the relative position of the helices and provide directional support. This support is effective in resisting the bending of the helix and changes to the secondary structure. Furthermore, we highlight that the lack of helical hydrogen bonds caused by helix kinks is a crucial reason for the differing rigidity of the monomer and its helices under various directions of external forces. Numerous studies have shown that the BAR domain plays a significant role in membrane bending, especially in liposome formation. [34, 55, 60–62].

LIST OF ABBREVIATIONS

BAR = Bin1/Amphiphysin/Rvs167

= Molecular Dynamics MD

SMD = Steered Molecular Dynamics

RMSD = Root Mean Square Deviation

TRFDA= Time-resolved Force Distribution Analysis

ETHICS APPROVAL AND **CONSENT** TO **PARTICIPATE**

Not applicable.

HUMAN AND ANIMAL RIGHTS

No humans/animals were used for studies that are the basis of this research.

CONSENT FOR PUBLICATION

Not applicable.

AVAILABILITY OF DATA AND MATERIALS

The data supporting the findings of the article are available at https://tinyurl.com/525t9kb4

FUNDING

This research was funded by the National Science Foundation Graduate Research Fellowship Program (Grant No. DGE-1939267) and the National Science Foundation (Grant No. 2137558). This work was also supported by the Substance Use Disorders Grand Challenge Pilot Research Award, the Research Allocations Committee (RAC) Award, the startup fund from the University of New Mexico, and the University of New Mexico Office of the Vice President for Research WeR1 Faculty Success Program. This work was supported by Student Research Grant (SRG) from the University of New Mexico, and the University of New Mexico of Graduate and Professional Student Association (GPSA).

CONFLICT OF INTEREST

The authors declare no competing financial interest.

ACKNOWLEDGEMENTS

Declared none.

SUPPLEMENTARY MATERIAL

Supplementary material with supporting information is available on the publisher's web site along with the published article.

REFERENCES

- [1] Tian, T.; Zhu, Y. L.; Zhou, Y. Y.; Liang, G. F.; Wang, Y. Y.; Hu, F. H.; Xiao, Z. D. Exosome Uptake through Clathrin-Mediated Endocytosis and Macropinocytosis and Mediating MiR-21 Delivery. J. Biol. Chem., 2014, 289 (32), 22258–22267.
- [2] Faille, D.; El-Assaad, F.; Mitchell, A. J.; Alessi, M. C.; Chimini, G.; Fusai, T.; Grau, G. E.; Combes, V. Endocytosis and Intracellular Processing of Platelet Microparticles by Brain Endothelial Cells. J. Cell. Mol. Med., 2012, 16 (8), 1731-1738.
- [3] Jorgensen, W. L.; Tirado-Rives, J. Potential Energy Functions for Atomic-Level Simulations of Water and Organic and Biomolecular Systems. Proceedings of the National Academy of Sciences of the United States of America. 2005, pp 6665–6670.
- [4] Zimmerberg, J.; Kozlov, M. M. How Proteins Produce Cellular Membrane Curvature. Nature Reviews Molecular Cell Biology. 2006, pp 9–19.
- Sivadon, P.; Bauer, F.; Aigle, M.; Crouzet, M. Actin [5] Cytoskeleton and Budding Pattern Are Altered in the Yeast Rvs161 Mutant: The Rvs161 Protein Shares

- Common Domains with the Brain Protein Amphiphysin. *MGG Mol. Gen. Genet.*, **1995**, *246* (4), 485–495.
- [6] Lichte, B.; Veh, R. W.; Meyer, H. E.; Kilimann, M. W. Amphiphysin, a Novel Protein Associated with Synaptic Vesicles. *EMBO J.*, 1992, 11 (7), 2521–2530.
- [7] Sakamuro, D.; Elliott, K. J.; Wechsler-Reya, R.; Prendergast, G. C. BIN1 Is a Novel MYC-Interacting Protein with Features of a Tumour Suppressor. *Nat. Genet.*, **1996**, *14* (1), 69–77.
- [8] Dharmalingam, E.; Haeckel, A.; Pinyol, R.; Schwintzer, L.; Koch, D.; Kessels, M. M.; Qualmann, B. F-BAR Proteins of the Syndapin Family Shape the Plasma Membrane and Are Crucial for Neuromorphogenesis. *J. Neurosci.*, **2009**, 29 (42), 13315–13327.
- [9] Kim, B. L.; Bu, W.; Wah, I. G.; Koh, E.; Siew, H. O.; Pawson, T.; Sudhaharan, T.; Ahmed, S. The Cdc42 Effector IRSp53 Generates Filopodia by Coupling Membrane Protrusion with Actin Dynamics. J. Biol. Chem., 2008, 283 (29), 20454–20472.
- [10] Krugmann, S.; Jordens, I.; Gevaert, K.; Driessens, M.; Vandekerckhove, J.; Hall, A. Cdc42 Induces Filopodia by Promoting the Formation of an IRSp53:Mena Complex. Curr. Biol., 2001, 11 (21), 1645–1655.
- [11] Ho, H. Y. H.; Rohatgi, R.; Lebensohn, A. M.; Le Ma; Li, J.; Gygi, S. P.; Kirschner, M. W. Toca-1 Mediates Cdc42-Dependent Actin Nucleation by Activating the N-WASP-WIP Complex. *Cell*, **2004**, *118* (2), 203–216.
- [12] Kamioka, Y.; Fukuhara, S.; Sawa, H.; Nagashima, K.; Masuda, M.; Matsuda, M.; Mochizuki, N. A Novel Dynamin-Associating Molecule, Formin-Binding Protein 17, Induces Tubular Membrane Invaginations and Participates in Endocytosis. *J. Biol. Chem.*, 2004, 279 (38), 40091–40099.
- [13] Salazar, M. A.; Kwiatkowski, A. V.; Pellegrini, L.; Cestra, G.; Butler, M. H.; Rossman, K. L.; Serna, D. M.; Sondek, J.; Gertler, F. B.; De Camilli, P. Tuba, a Novel Protein Containing Bin/Amphiphysin/Rvs and Dbl Homology Domains, Links Dynamin to Regulation of the Actin Cytoskeleton. *J. Biol.* Chem., 2003, 278 (49), 49031–49043.
- [14] Liu, S.; Xiong, X.; Zhao, X.; Yang, X.; Wang, H. F-BAR Family Proteins, Emerging Regulators for Cell Membrane Dynamic Changes From Structure to Human Diseases. *Journal of Hematology and Oncology*. 2015, p 47.
- [15] Bi, X.; Corpina, R. A.; Goldberg, J. Structure of the Sec23/24-Sar1 Pre-Budding Complex of the COPII Vesicle Coat. *Nature*, **2002**, *419* (6904), 271–277.

- [16] Farsad, K.; Ringstad, N.; Takei, K.; Floyd, S. R.; Rose, K.; De Camilli, P. Generation of High Curvature Membranes Mediated by Direct Endophilin Bilayer Interactions. *J. Cell Biol.*, **2001**, *155* (2), 193–200.
- [17] Masuda, M.; Takeda, S.; Sone, M.; Ohki, T.; Mori, H.; Kamioka, Y.; Mochizuki, N. Endophilin BAR Domain Drives Membrane Curvature by Two Newly Identified Structure-Based Mechanisms. *EMBO J.*, 2006, 25 (12), 2889–2897.
- [18] Gallop, J. L.; Jao, C. C.; Kent, H. M.; Butler, P. J. G.; Evans, P. R.; Langen, R.; McMahon, H. T. Mechanism of Endophilin N-BAR Domain-Mediated Membrane Curvature. *EMBO J.*, 2006, 25 (12), 2898–2910.
- [19] Peter, B. J.; Kent, H. M.; Mills, I. G.; Vallis, Y.; Butler, P. J. G.; Evans, P. R.; McMahon, H. T. BAR Domains as Sensors of Membrane Curvature: The Amphiphysin BAR Structure. *Science* (80-.)., **2004**, 303 (5657), 495–499.
- [20] Richnau, N.; Fransson, Å.; Farsad, K.; Aspenström, P. RICH-1 Has a BIN/Amphiphysin/Rvsp Domain Responsible for Binding to Membrane Lipids and Tubulation of Liposomes. *Biochem. Biophys. Res.* Commun., 2004, 320 (3), 1034–1042.
- [21] Weissenhorn, W. Crystal Structure of the Endophilin-A1 BAR Domain. *J. Mol. Biol.*, **2005**, *351* (3), 653–661.
- [22] Zhang, B.; Zelhof, A. C. Amphiphysins: Raising the BAR for Synaptic Vesicle Recycling and Membrane Dynamics. *Traffic*, **2002**, *3* (7), 452–460.
- [23] Stevens, A. O.; Kazan, I. C.; Ozkan, B.; He, Y. Investigating the Allosteric Response of the PICK1 PDZ Domain to Different Ligands with All-atom Simulations. *Protein Sci.*, 2022, 31 (12), e4474.
- [24] Hendrix, E.; Motta, S.; Gahl, R. F.; He, Y. Insight into the Initial Stages of the Folding Process in Onconase Revealed by UNRES. *J. Phys. Chem. B*, **2022**, *126* (40), 7934–7942.
- [25] Hendrix, E.; Motta, S.; Gahl, R. F.; He, Y. Insight into the Initial Stages of the Folding Process in Onconase Revealed by UNRES. *J. Phys. Chem. B*, **2022**, *126* (40), 7934–7942.
- [26] Li, T.; Motta, S.; Stevens, A. O.; Song, S.; Hendrix, E.; Pandini, A.; He, Y. Recognizing the Binding Pattern and Dissociation Pathways of the P300 Taz2-P53 TAD2 Complex. *J. Am. Chem. Soc.*, **2022**, *2* (8), 1935–1945.
- [27] Stevens, A. O.; He, Y. Residue-Level Contact Reveals Modular Domain Interactions of PICK1 Are Driven by Both Electrostatic and Hydrophobic Forces. *Front. Mol. Biosci.*, **2021**, *7*, 485.
- [28] Li, T.; Stevens, A. O.; Gil Pineda, L. I.; Song, S.; Ameyaw Baah, C. A.; He, Y. Changes in Structure

- and Flexibility of P53 TAD2 upon Binding to P300 Taz2. J. Theor. Comput. Chem., **2020**, 19 (4).
- [29] Gil Pineda, L. I.; Milko, L. N.; He, Y. Performance of CHARMM36m with Modified Water Model in Simulating Intrinsically Disordered Proteins: A Case Study. *Biophys. Reports*, **2020**, *6* (2–3), 80–87.
- [30] He, Y.; Maisuradze, G. G.; Yin, Y.; Kachlishvili, K.; Rackovsky, S.; Scheraga, H. A. Sequence-, Structure-, and Dynamics-Based Comparisons of Structurally Homologous CheY-like Proteins. *Proc. Natl. Acad. Sci. U. S. A.*, 2017, 114 (7), 1578–1583.
- [31] He, Y.; Mozolewska, M. A.; Krupa, P.; Sieradzan, A. K.; Wirecki, T. K.; Liwo, A.; Kachlishvili, K.; Rackovsky, S.; Jagieła, D.; Ślusarz, R.; et al. Lessons from Application of the UNRES Force Field to Predictions of Structures of CASP10 Targets. Proc. Natl. Acad. Sci. U. S. A., 2013, 110 (37), 14936–14941.
- [32] He, Y.; Liwo, A.; Weinstein, H.; Scheraga, H. A. PDZ Binding to the BAR Domain of PICK1 Is Elucidated by Coarse-Grained Molecular Dynamics. *J. Mol. Biol.*, **2011**, *405* (1), 298–314.
- [33] Blood, P. D.; Voth, G. A. Direct Observation of Bin/Amphiphysin/Rvs (BAR) Domain-Induced Membrane Curvature by Means of Molecular Dynamics Simulations. *Proc. Natl. Acad. Sci. U. S. A.*, **2006**, *103* (41), 15068–15072.
- [34] Blood, P. D.; Swenson, R. D.; Voth, G. A. Factors Influencing Local Membrane Curvature Induction by N-BAR Domains as Revealed by Molecular Dynamics Simulations. *Biophys. J.*, 2008, 95 (4), 1866–1876.
- [35] Han, D. S. & Weinstein, H. Auto-Inhibition in the Multi-Domain Protein PICK 1 Revealed by Dynamic Models of Its Quaternary Structure. *Biophys. J.*, **2008**, *94*, 67–76.
- [36] Tarricone, C.; Xiao, B.; Justin, N.; Walker, P. A.; Rittinger, K.; Gamblin, S. J.; Smerdon, S. J. The Structural Basis of Arfaptin-Mediated Cross-Talk between Rac and Arf Signalling Pathways. *Nature*, **2001**, *411* (6834), 215–219.
- [37] Jorgensen, W. L.; Chandrasekhar, J.; Madura, J. D.; Impey, R. W.; Klein, M. L. Comparison of Simple Potential Functions for Simulating Liquid Water. *J. Chem. Phys.*, **1983**, *79* (2), 926–935.
- [38] Lee, J.; Cheng, X.; Swails, J. M.; Yeom, M. S.; Eastman, P. K.; Lemkul, J. A.; Wei, S.; Buckner, J.; Jeong, J. C.; Qi, Y.; et al. CHARMM-GUI Input Generator for NAMD, GROMACS, AMBER, OpenMM, and CHARMM/OpenMM Simulations Using the CHARMM36 Additive Force Field. *J. Chem. Theory Comput.*, **2016**, *12* (1), 405–413.
- [39] Huang, J.; MacKerell, A. D. CHARMM36 All-Atom Additive Protein Force Field: Validation Based on

- Comparison to NMR Data. *J. Comput. Chem.*, **2013**, *34* (25), 2135–2145.
- [40] Humphrey, W.; Dalke, A.; Schulten, K. VMD: Visual Molecular Dynamics. *J. Mol. Graph.*, **1996**, *14* (1), 33–38.
- [41] Pettersen, E. F.; Goddard, T. D.; Huang, C. C.; Couch, G. S.; Greenblatt, D. M.; Meng, E. C.; Ferrin, T. E. UCSF Chimera A Visualization System for Exploratory Research and Analysis. *J. Comput. Chem.*, **2004**, *25* (13), 1605–1612.
- [42] Berendsen, H. J. C.; van der Spoel, D.; van Drunen, R. GROMACS: A Message-Passing Parallel Molecular Dynamics Implementation. *Comput. Phys. Commun.*, **1995**, *91* (1–3), 43–56.
- [43] Abraham, M. J.; Murtola, T.; Schulz, R.; Páll, S.; Smith, J. C.; Hess, B.; Lindah, E. Gromacs: High Performance Molecular Simulations through Multi-Level Parallelism from Laptops to Supercomputers. *SoftwareX*, **2015**, *1*–2, 19–25.
- [44] Hess, B.; Bekker, H.; Berendsen, H. J. C.; Fraaije, J. G. E. M. LINCS: A Linear Constraint Solver for Molecular Simulations. *J. Comput. Chem.*, 1997, 18 (12), 1463–1472.
- [45] Darden, T.; York, D.; Pedersen, L. Particle Mesh Ewald: An N·log(N) Method for Ewald Sums in Large Systems. *J. Chem. Phys.*, **1993**, *98* (12), 10089–10092.
- [46] Essmann, U.; Perera, L.; Berkowitz, M. L.; Darden, T.; Lee, H.; Pedersen, L. G. A Smooth Particle Mesh Ewald Method. *J. Chem. Phys.*, **1995**, *103* (19), 8577–8593.
- [47] Apostolakis, J.; Ferrara, P.; Caflisch, A. Calculation of Conformational Transitions and Barriers in Solvated Systems: Application to the Alanine Dipeptide in Water. *J. Chem. Phys.*, **1999**, *110* (4), 2099–2108.
- [48] Costescu, B. I.; Gräter, F. Time-Resolved Force Distribution Analysis. *BMC Biophys.*, **2013**, *6* (1), 5.
- [49] Stacklies, W.; Seifert, C.; Graeter, F. Implementation of Force Distribution Analysis for Molecular Dynamics Simulations. *BMC Bioinformatics*, **2011**, *12* (1), 1–5.
- [50] Abraham, M.; Hess, B.; Spoel, D. van der; Lindahl, E. GROMACS User Manual-5.0.7. *Www.Gromacs.Org*, **2015**.
- [51] Eisenhaber, F.; Lijnzaad, P.; Argos, P.; Sander, C.; Scharf, M. The Double Cubic Lattice Method: Efficient Approaches to Numerical Integration of Surface Area and Volume and to Dot Surface Contouring of Molecular Assemblies. *J. Comput. Chem.*, **1995**, *16* (3), 273–284.
- [52] Kabsch, W.; Sander, C. Dictionary of Protein Secondary Structure: Pattern Recognition of Hydrogen-Bonded and Geometrical Features.

- Biopolymers, 1983, 22 (12), 2577–2637.
- [53] Wilman, H. R.; Shi, J.; Deane, C. M. Helix Kinks Are Equally Prevalent in Soluble and Membrane Proteins. *Proteins Struct. Funct. Bioinforma.*, **2014**, 82 (9), 1960–1970.
- [54] Laskowski, R. A.; Swindells, M. B. LigPlot+: Multiple Ligand-Protein Interaction Diagrams for Drug Discovery. *J. Chem. Inf. Model.*, **2011**, *51* (10), 2778–2786.
- [55] Yu, H.; Schulten, K. Membrane Sculpting by F-BAR Domains Studied by Molecular Dynamics Simulations. *PLoS Comput. Biol.*, **2013**, *9* (1), 1002892.
- [56] Mahmood, M. I.; Noguchi, H.; Okazaki, K. ichi. Curvature Induction and Sensing of the F-BAR Protein Pacsin1 on Lipid Membranes via Molecular Dynamics Simulations. Sci. Rep., 2019, 9 (1), 1–11.
- [57] Blundell, T.; Barlow, D.; Borkakoti, N.; Thornton, J. Solvent-Induced Distortions and the Curvature of α -Helices. *Nature*, **1983**, *306* (5940), 281–283.
- [58] Langelaan, D. N.; Wieczorek, M.; Blouin, C.; Rainey, J. K. Improved Helix and Kink Characterization in Membrane Proteins Allows Evaluation of Kink Sequence Predictors. *J. Chem. Inf. Model.*, **2010**, *50* (12), 2213–2220.
- [59] Law, E. C.; Wilman, H. R.; Kelm, S.; Shi, J.; Deane, C. M. Examining the Conservation of Kinks in Alpha Helices. *PLoS One*, **2016**, *11* (6), e0157553.
- [60] Mim, C.; Cui, H.; Gawronski-Salerno, J. A.; Frost, A.; Lyman, E.; Voth, G. A.; Unger, V. M. Structural Basis of Membrane Bending by the N-BAR Protein Endophilin. *Cell*, 2012, 149 (1), 137–145.
- [61] Yin, Y.; Arkhipov, A.; Schulten, K. Simulations of Membrane Tubulation by Lattices of Amphiphysin N-BAR Domains. *Structure*, 2009, 17 (6), 882–892.
- [62] Arkhipov, A.; Yin, Y.; Schulten, K. Membrane-Bending Mechanism of Amphiphysin N-BAR Domains. *Biophys. J.*, **2009**, *97* (10), 2727–2735.